https://doi.org/10.5194/egusphere-2026-2792
Preprint. Discussion started: 21 July 2026

Measurement report: Seasonal dynamics and driving factors of aqueous-phase photooxidants in atmospheric particles: Implications for wintertime SOA formation

Min Cai[1,2], Qing Yu[1,2], Ke Xin[1,2], Mushtaq Ahmad[1,3], Jing Chen[1,2]

[1] State Key Joint Laboratory of Environment Simulation and Pollution Control, School of Environment, Beijing Normal University, Beijing 100875, China

[2] Center for Atmospheric Environmental Studies, Beijing Normal University, Beijing 100875, China

[3] National Astronomical Research Institute of Thailand, Chiang Mai 50180, Thailand

Correspondence to: Jing Chen (jingchen@bnu.edu.cn)

https://doi.org/10.5194/egusphere-2026-2792
Preprint. Discussion started: 21 July 2026

Abstract. Aqueous-phase oxidation processes significantly promote secondary organic aerosol (SOA) formation, driven primarily by photooxidants including hydroxyl radical (·OH), singlet oxygen ($^1O_2$*), and organic triplet excited states (^{3}C*). However, seasonal variations and driving factors of these oxidants in atmospheric aqueous phases remain poorly understood. In this study, we quantified the steady-state concentrations of ·OH, $^1O_2$*, and ^{3}C* in $PM_{2.5}$ extracts under simulated solar irradiation, and estimated their ranges in ambient aerosol water. The results show that [·OH] exhibited no significant seasonal variation, whereas [$^1O_2$*] and [^{3}C*] displayed distinct seasonal variations of winter > autumn > summer. All three oxidants correlated strongly with water-soluble organic compounds (WSOC), especially biomass burning-derived WSOC. By extrapolating the fitted relationships between oxidant concentrations ([·OH], [$^1O_2$*], and [^{3}C*]) and extract concentrations to ambient conditions, their ranges in ambient aerosol water were estimated as [·OH] = (1.0–5.4) × 10^{-14} M, [$^1O_2$*] = (2.3–61.9) × 10^{-11} M, and [^{3}C*] = (1.6–35.8) × 10^{-12} M. The relative contributions of the three photooxidants to aqueous-phase oxidation of typical organic precursors revealed the dominant role of ^{3}C*-mediated reactions in ambient aerosol water, even at low temperatures. This work thus resolves the winter SOA underestimation in current model studies by demonstrating the critical yet overlooked role of ^{3}C*-mediated aqueous-phase oxidation.

Keywords: Organic triplet excited states; Singlet oxygen; WSOC; SOA; Biomass burning.

https://doi.org/10.5194/egusphere-2026-2792
Preprint. Discussion started: 21 July 2026

Graphical abstract:

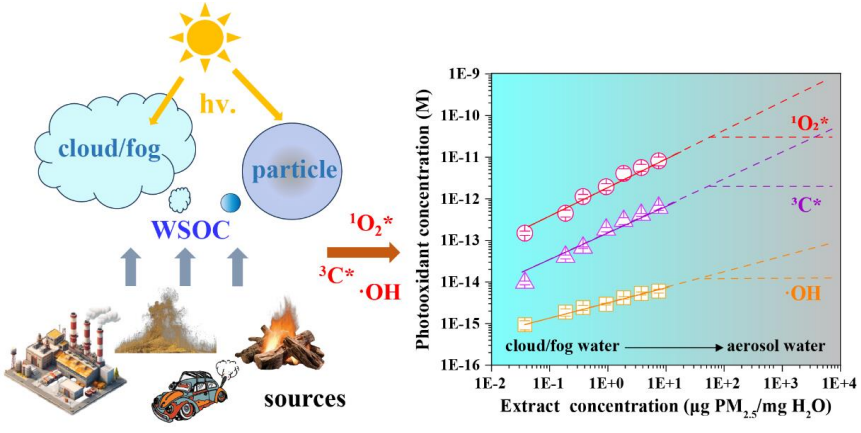

https://doi.org/10.5194/egusphere-2026-2792
Preprint. Discussion started: 21 July 2026

1 Introduction

The atmospheric aqueous phase, including cloud/fog water and aerosol liquid water, serves as a critical medium for photochemical reactions of various atmospheric chemical species (Sun et al., 2025). Numerous reactions that are difficult to initiate or proceed slowly in the gas phase can occur or accelerate in the aqueous phase (Li et al., 2021; Wang et al., 2022a). Extensive research has demonstrated that aqueous-phase oxidation processes contribute substantially to the formation and aging of secondary organic aerosols (SOA). Globally, aqueous-phase SOA contributes at levels comparable to gas-phase SOA; in regions with high humidity and severe pollution, its importance may even surpass gas-phase SOA (Wang et al., 2022b; Wang et al., 2023). Furthermore, incorporating aqueous-phase SOA into atmospheric models significantly improves SOA simulation performance (Al-Abadleh, 2024; Fahey et al., 2025). Thus, investigating aqueous-phase SOA oxidation mechanisms would enhance understanding of SOA formation processes, reduce discrepancies between simulated and observed SOA concentrations, and improve model predictive accuracy for SOA generation.

Aqueous-phase oxidation of SOA is driven by oxidants present in the atmospheric aqueous phase, primarily including hydroxyl radical (·OH), singlet oxygen ($^1O_2$*), and organic triplet excited states (^{3}C*) (Tilgner et al., 2021; Li et al., 2023; Jiang et al., 2024). Currently, ·OH in atmospheric liquid water has been extensively studied. Sources of ·OH in the atmospheric aqueous phase include gas-phase transport, photolysis of nitrite (NO_2^-), nitrate (NO_3^-), hydrogen peroxide (H_2O_2), and organic peroxides, photo-Fenton reactions, and photoexcitation of water-soluble organic

https://doi.org/10.5194/egusphere-2026-2792
Preprint. Discussion started: 21 July 2026

compounds (WSOC); and the major sink for ·OH is organic matter within aqueous droplets (Tong et al., 2020; Dwinandha et al., 2022; Ervens, 2022). Based on field observations and laboratory studies, ·OH concentrations in the atmospheric aqueous phase are generally relatively low, typically 10^{-16}–10^{-15} mol·L^{-1} in cloud water and 10^{-13}–10^{-12} mol·L^{-1} in aerosol water (Kaur and Anastasio, 2017; Ma et al., 2023) . However, ·OH exhibits exceptionally high reactivity, capable of reacting with virtually all organic compounds in the atmosphere (Kroflič et al., 2020; Mitra et al., 2022).

Certain organic compounds can absorb solar radiation and become photoexcited to form reactive triplet excited states (^{3}C*). ^{3}C* constitutes effective oxidants capable of generating other oxidants such as $^1O_2$* and H_2O_2, or oxidizing organic compounds directly through electron transfer reactions (Leresche et al., 2021; Mabato et al., 2021) . Laboratory studies have demonstrated that ^{3}C* plays an important role in the aqueous-phase oxidation of phenolic compounds that are abundantly emitted from biomass burning (Mabato et al., 2022; Mabato et al., 2023). Compared to ·OH, research on ^{3}C* in the atmospheric aqueous phase remains relatively limited. Since ^{3}C* is not a single oxidant but comprises multiple species with diverse reactivities, determination of its steady-state concentration in atmospheric liquid water presents a big challenge (Gemayel et al., 2021; Li et al., 2023). Roughly, the concentrations of ^{3}C* in the atmospheric aqueous phase are slightly higher than ·OH: in cloud droplets, ^{3}C* concentrations range from 10^{-15} to 10^{-13} mol·L^{-1}, whereas in aerosol water, ^{3}C* concentrations are substantially higher, approximately 10^{-13}–10^{-11} mol·L^{-1} (Kaur and Anastasio, 2018; Ma et al., 2023).

https://doi.org/10.5194/egusphere-2026-2792
Preprint. Discussion started: 21 July 2026

$^3C^*$ can transfer energy to dissolved oxygen, forming another important oxidant, $^1O_2^*$ (Gerritz et al., 2024; Zhang et al., 2024). Despite its substantially lower reactivity compared to ·OH, $^1O_2^*$ reacts rapidly with electron-rich organic compounds such as phenols, polycyclic aromatic hydrocarbons, amino acids, and reduced sulfur compounds (Kaur and Anastasio, 2017; Ma et al., 2024). Moreover, laboratory simulation studies have revealed that $^1O_2^*$ concentrations in cloud droplets and aerosol liquid water can exceed ·OH concentrations by 2–3 orders of magnitude: $^1O_2^*$ concentrations in cloud droplets range from 10^{-14} to 10^{-12} mol·L^{-1}, whereas in aerosol liquid water, $^1O_2^*$ concentrations can reach 10^{-10} mol·L^{-1}, representing the highest concentration among the three oxidants (Kaur and Anastasio, 2017; Ma et al., 2023). Given its relatively high concentrations, $^1O_2^*$ also represents a potentially competitive oxidant in the atmospheric aqueous phase.

Although ·OH, $^1O_2^*$, and $^3C^*$ play important roles in the aqueous-phase transformation of atmospheric species, measurements of their steady-state concentrations in the atmospheric aqueous phase remain scarce, and understanding of their seasonal variation characteristics and influencing factors is limited. In this study, we determined the steady-state concentrations of the three major photochemical oxidants (·OH, $^1O_2^*$, and $^3C^*$) in $PM_{2.5}$ extracts under simulated solar irradiation, based on $PM_{2.5}$ samples collected in urban Beijing across different seasons. The objectives of this work were to: (1) compare the steady-state concentrations of ·OH, $^1O_2^*$, and $^3C^*$ in $PM_{2.5}$ extracts across different seasons; (2) investigate their influencing factors; and (3) evaluate their contributions to the aqueous-phase oxidation of typical precursors and

https://doi.org/10.5194/egusphere-2026-2792
Preprint. Discussion started: 21 July 2026

SOA formation. This study provides significant implications for advancing our understanding of aerosol aqueous-phase oxidation mechanisms in the atmosphere.

2 Experimental

2.1 Preparation and photooxidation of $PM_{2.5}$ extracts

Steady-state concentrations of photooxidants were determined in irradiated aqueous $PM_{2.5}$ extracts, using $PM_{2.5}$ samples collected in a mixed traffic–residential–commercial zone of urban Beijing in summer (July), autumn (October), and winter (January). Details of the sampling process can be found in our previous study (Yu et al., 2021a). To investigate the effect of extract concentration on oxidant steady-state concentrations, a high-concentration $PM_{2.5}$ stock extract was prepared and subsequently subjected to serial dilution. The surface of a defined area of each $PM_{2.5}$-loaded filter was carefully peeled and cut into small pieces, soaked in 10 mL ultrapure water (18.2 MΩ·cm), and subjected to ultrasonic extraction for 20 minutes. This extraction procedure was repeated twice. The combined extract was then filtered through a 0.45 μm PTFE syringe filter and stored at 4 °C in the dark for further use. The concentration of the stock extract was around 7.5 μg $PM_{2.5}$/mg H_2O, approximately an order of magnitude higher than that (0.84 μg $PM_{2.5}$/mg H_2O) obtained in previous research (Kaur et al., 2019). Serial dilutions were then prepared by diluting the stock solution 1-fold (neat), 2-fold, 4-fold, 8-fold, 20-fold, 40-fold, and 200-fold with ultrapure water.

The aqueous-phase photochemical experiments were conducted in a custom-built reaction system, in which a 500 W long-arc xenon lamp was used to simulate tropospheric solar radiation. Details of the reaction system can be found in the

https://doi.org/10.5194/egusphere-2026-2792
Preprint. Discussion started: 21 July 2026

supplement (Sect. S1 and Fig. S1). Steady-state concentrations of ·OH, $^1O_2$*, and ^3C* were quantified for each $PM_{2.5}$ extract solution. All measurements were performed in triplicate, and mean values are reported.

2.2 Determination of photooxidants

2.2.1 Formation rate, loss rate, and steady-state concentration of ·OH

The formation rate (P_{OH}), loss rate constant (k'_{OH}), and steady-state concentration ([·OH]) of ·OH generated from the photoreaction of aqueous $PM_{2.5}$ extracts were quantified using a competitive kinetic method with benzoic acid /benzoate (BA/BA^-) as the probes. 5 mL aliquots of the $PM_{2.5}$ extract were taken and added with sodium benzoate solution to achieve final sodium benzoate concentrations of 20 μM, 30 μM, 60 μM, and 200 μM, respectively. The mixtures were then exposed to xenon lamp irradiation and 200 μL of each mixture was withdrawn for every 20 min to quantify the generated 4-hydroxybenzoic acid (4-OHBA) concentration using high-performance liquid chromatography (HPLC). The slope of the linear regression of [4-OHBA] versus irradiation time was designated as k_p. With mixtures of different initial concentrations of benzoate, a double-reciprocal plot was constructed with $1/(BA/BA^-)$ as the abscissa and $1/k_p$ as the ordinate. Linear regression of this plot yielded a slope and y intercept, from which $P_{OH,EXP}$ ($M \cdot s^{-1}$), k'_{OH} (s^{-1}), and $[\cdot OH]_{EXP}$ (M) can be calculated via the following equations (Arakaki et al., 2013; Gweme and Styler, 2024):

$$P_{OH,EXP} = \frac{1}{y\ intercept \times Yield} \quad (1)$$

$$k'_{OH} = k_0 \left(\frac{slope}{y\ intercept}\right) \quad (2)$$

$$[\cdot OH]_{EXP} = \frac{1}{k_0 \times slope \times Yield} \quad (3)$$

https://doi.org/10.5194/egusphere-2026-2792
Preprint. Discussion started: 21 July 2026

where *Yield* represents the formation yield of 4-OHBA from the reaction of ·OH with the probes (0.17), and k_0 is the second-order rate constant for the reaction between ·OH and BA/BA^- ($M^{-1}\cdot s^{-1}$), which can be calculated as follows:

$$k_0 = \alpha_{BAH} k_{BAH,OH} + \alpha_{BA^-} k_{BA^-,OH} \quad (4)$$

Here, $k_{BAH,OH}$ and $k_{BA^-,OH}$ denote the second-order rate constants for the reactions of ·OH with BA (4.3×10^9 $M^{-1}\cdot s^{-1}$) and BA^- (5.9×10^9 $M^{-1}\cdot s^{-1}$), respectively; α_{BAH} and α_{BA^-} represent the molar fractions of BA and BA^- under the solution pH condition, determined from the Henderson–Hasselbalch equation:

$$pH_{sample} = pK_a + lg\frac{[BA^-]}{[BAH]} \quad (5)$$

where pH_{sample} is the pH of the solution, and pK_a of BA is 4.19.

$P_{OH,EXP}$ and $[\cdot OH]_{EXP}$ were then corrected to obtain P_{OH} and [·OH] using the internal light screening factor (S_λ) of the extract solution, which can be calculated as follows:

$$S_\lambda = \frac{\sum_{300}^{450}[(1-10^{-\alpha_\lambda l})\times I_\lambda]}{\sum_{300}^{450}[(2.303\times\alpha_\lambda l)\times I_\lambda]} \quad (6)$$

where α_λ (cm^{-1}) is the absorbance of the solution over the wavelength range of 300–450 nm, measured by UV–vis spectrophotometry with a 1 cm path length; l (cm) is the depth of the reaction solution; and I_λ represents the actinic flux of the xenon lamp within the 300–450 nm range.

To further investigate the influence of NO_2^- and NO_3^- photolysis on ·OH generation in this study, the formation rates of ·OH from NO_2^- and NO_3^- photolysis were also calculated using the following equations:

$$P_{OH,NO2-} = j_{NO2-\rightarrow OH} \times [NO_2^-] \quad (7)$$

https://doi.org/10.5194/egusphere-2026-2792
Preprint. Discussion started: 21 July 2026

$$P_{OH,NO3-} = j_{NO3-\rightarrow OH} \times [NO_3^-] \quad (8)$$

where $[NO_2^-]$ and $[NO_3^-]$ denote the concentrations of NO_2^- and NO_3^- in $PM_{2.5}$ extract solution (M), respectively; $j_{NO2-\rightarrow OH}$ and $j_{NO3-\rightarrow OH}$ represent the photolysis rate constants for NO_2^- and NO_3^- under the experimental conditions, with $j_{NO2-\rightarrow OH} = 3.0\times10^{-5}$ s^{-1} and $j_{NO3-\rightarrow OH} = 1.6\times10^{-7}$ s^{-1}.

2.2.2 Steady-state concentration of $^1O_2$*

The steady-state concentration of $^1O_2$* was determined using furfuryl alcohol (FFA) and deuterium oxide (D_2O). Each $PM_{2.5}$ extract solution was divided into two equal aliquots, which were then diluted with H_2O and D_2O, respectively. FFA was then added to both aliquots to achieve an initial concentration of approximately 10 μM; this low initial concentration was maintained to avoid depletion of $^1O_2$* during the experiment. The FFA degradation under xenon lamp irradiation was quantified by HPLC at 10-minute intervals, which followed pseudo-first-order kinetics. For all samples, the rate constant for FFA decay in D_2O-diluted extract (k_{D2O}, s^{-1}) exceeded that in H_2O-diluted extract (k_{H2O}, s^{-1}), because H_2O was the primary sink for $^1O_2$*. The first-order decay rate constant of $^1O_2$* in H_2O ($k'_{H2O} = 2.2 \times 10^5$ s^{-1}) is approximately 14-fold greater than that in D_2O ($k'_{D2O} = 1.6 \times 10^4$ s^{-1}). The steady-state concentration of $^1O_2$* ($[^1O_2^*]$, M) was then calculated from the difference in FFA decay rate constants between H_2O- and D_2O-diluted extracts (Kaur et al., 2019):

$$[^1O_2^*]_{EXP} = \frac{k_{D_2O} - k_{H_2O}}{D \times k_{FFA+^1O_2} \times \left(\frac{k'_{H_2O}}{k'_{H_2O}\chi_{H_2O} + k'_{D_2O}\chi_{D_2O}} - 1 \right)} \quad (9)$$

where D represents the dilution factor, defined as the ratio of undiluted solution volume to the final diluted solution volume ($D = 0.5$ in this study); $k_{FFA+^1O_2}$ is the second-order

https://doi.org/10.5194/egusphere-2026-2792
Preprint. Discussion started: 21 July 2026

rate constant for the reaction between FFA and $^1O_2$* (1.06×10^8 $M^{-1} \cdot s^{-1}$ at 25 °C); and χ_{H2O} and χ_{D2O} denote the mole fractions of H_2O and D_2O in the irradiated solution, respectively. The resulting $[^1O_2^*]_{EXP}$ values were subsequently corrected to obtain $[^1O_2^*]$ using S_λ (Eq. 6) of the extract solution.

2.2.3 Steady-state concentration of ^{3}C*

^{3}C* is virtually a mixture of reactive organic species with varying chemical structures and reactivities. In this study, the steady-state concentration of ^{3}C* in irradiated $PM_{2.5}$ extract solution was estimated using a dual-probe technique developed by Kaur and Anastasio (2018). The two probes were 2,6-dimethoxyphenol (SYR) and methyl jasmonate (MeJA), with the former being an electron-rich phenol that reacts rapidly with a broad range of ^{3}C* species, and the latter exhibiting lower but more variable reactivity with different ^{3}C*s.

During the experiment, each sample solution was divided into two equal aliquots, to which SYR and MeJA were added to achieve initial concentrations of 0.5–1 ppm and 1 ppm, respectively. The low probe concentrations were maintained to prevent depletion of ^{3}C* during irradiation. The SYR and MeJA concentrations during irradiation were quantified by HPLC at 10-minute and 20-minute intervals, respectively. The decay of both probes followed pseudo-first-order kinetics, with the observed rate constant (k'_{Probe}, s^{-1}) determined from the absolute value of the slope of the linear regression of $\ln([Probe]_t/[Probe]_0)$ versus irradiation time (t). In addition to the reaction with ^{3}C*, both SYR and MeJA were susceptible to oxidation by other photooxidants, such as ·OH and $^1O_2$*. Therefore, the observed probe decay rate constant can be

https://doi.org/10.5194/egusphere-2026-2792
Preprint. Discussion started: 21 July 2026

expressed as (Kaur et al., 2019):

$$k'_{Probe} = k_{Probe+OH}[\cdot OH] + k_{Probe+^1O_2*}[^1O_2*] + \sum\left(k_{Probe+^3C_i^*}[^3C_i^*]\right) + \sum(k_{Probe+Other}[Other]) + j_{Probe} \quad (10)$$

where $k_{Probe+OH}$, $k_{Probe+^1O_2*}$, $k_{Probe+^3C_i^*}$ and $k_{Probe+Other}$ represent the second-order reaction rate constants for the reactions of the probe with ·OH, $^1O_2$*, ^{3}C* and other oxidants (such as $HO_2\cdot/\cdot O_2^-$, O_3, $\cdot CO_3^-$), respectively; [·OH], [$^1O_2$*], [^{3}C*$_i$], and [Other] denote the steady-state concentrations of the corresponding oxidants in the extract; and j_{Probe} is the first-order photolysis rate constant of the probe (s^{-1}). The literature values of the rate constants are: k_{SYR+OH} = 2.6 × 10^{10} M^{-1} s^{-1}, $k_{MeJA+OH}$ = 6.7 × 10^9 M^{-1} s^{-1}, $k_{SYR+^1O_2*}$ = 3.6 × 10^7 M^{-1} s^{-1}, and $k_{MeJA+^1O_2*}$ = 6.0 × 10^5 M^{-1} s^{-1}. And the first-order photolysis rate constants of the two probes were experimentally determined as j_{SYR} = 4.1 × 10^{-6} s^{-1} and j_{MeJA} = 2.8 × 10^{-7} s^{-1}. Given the negligible contribution of other oxidants to probe consumption, Σ($k_{Probe+Other}$[Other]) was omitted. Then, the first-order rate constants for reaction of ^{3}C* with SYR and MeJA (k'$_{SYR,3C*}$ and k'$_{MeJA,3C*}$) can be calculated as follows:

$$k'_{Probe,^3C*} = \sum\left(k_{Probe+^3C_i^*}[^3C_i^*]\right) = k'_{Probe} - k_{Probe+OH}[\cdot OH] - k_{Probe+1O_2}[^1O_2*] - j_{Probe} \quad (11)$$

Meanwhile, the ^{3}C* concentration was roughly estimated using an "averaged" second-order rate constant ($k_{Probe+3C*}$) for the reaction between the probe and the ensemble of ^{3}C* species as follows:

$$\sum[^3C_i^*]_{Probe} \approx \frac{k'_{Probe,^3C*}}{k_{Probe+^3C*}} \quad (12)$$

To determine $k_{Probe+3C*}$ in Eq. (12), four model compounds were employed in this

https://doi.org/10.5194/egusphere-2026-2792
Preprint. Discussion started: 21 July 2026

work, including 2-acetonaphthone (2-AN), 3'-methoxyacetophenone (3-MAP), 3,4-dimethoxybenzaldehyde (DMB), and benzophenone (BP). Previous studies have demonstrated that highly reactive ^3C_i* species exhibit rapid reaction rates with both SYR and MeJA, resulting in a small ratio of second-order rate constants ($k_{SYR+3Ci*}/k_{MeJA+3Ci*}$); conversely, less reactive ^3C_i* species show greater disparity in reaction rates with SYR versus MeJA, yielding larger $k_{SYR+3Ci*}/k_{MeJA+3Ci*}$ values (Kaur and Anastasio, 2018). Thus, the ratio of $k_{SYR+3C*}/k_{MeJA+3C*}$ can serve as a qualitative indicator of the average reactivity of the ^{3}C* mixture. For the four model compounds, the ratios of second-order rate constants with the two probes for ^{3}2-AN*, ^{3}3MAP*, ^{3}DMB* and ^{3}BP* are 100, 32, 8.5, and 1.7, respectively. Thus, the reactivity range of ^{3}C* generated from these model compounds upon irradiation encompasses the typical reactivity spectrum of ^{3}C* in environmental samples.

After the ratio of first-order rate constants ($k'_{SYR,\ 3C*}/k'_{MeJA,\ 3C*}$) for each sample solution was calculated, the two model ^{3}C* species ($^3C_1$* and $^3C_2$*) whose reactivity ratios ($k_{SYR+3C*}/k_{MeJA+3C*}$) were closest to the sample ratio were identified as the "best-match" model species. Then the following equations were applied to calculate the fractional contributions of model species $^3C_1$* and $^3C_2$*:

$$\frac{k'_{SYR,^3C^*}}{k'_{MeJA,^3C^*}} \approx \frac{k_{SYR+^3C^*}[^3C^*]}{k_{MeJA+^3C^*}[^3C^*]} = \frac{k_{SYR+^3C^*}}{k_{MeJA+^3C^*}} = \frac{\chi_{^3C_1^*} \times k_{SYR+^3C_1^*} + \chi_{^3C_2^*} \times k_{SYR+^3C_2^*}}{\chi_{^3C_1^*} \times k_{MeJA+^3C_1^*} + \chi_{^3C_2^*} \times k_{MeJA+^3C_2^*}} \quad (13)$$

$$\chi_{^3C_1^*} + \chi_{^3C_2^*} = 1 \quad (14)$$

where $\chi_{^3C_1^*}$ and $\chi_{^3C_2^*}$ denote the fractional contributions of model species $^3C_1$* and $^3C_2$*, respectively. According to the calculated $\chi_{^3C_1^*}$ and $\chi_{^3C_2^*}$ values, the "averaged" second-order rate constant ($k_{Probe+3C*}$) for the reaction between the probe and ^{3}C* in the

https://doi.org/10.5194/egusphere-2026-2792
Preprint. Discussion started: 21 July 2026

sample solution can be estimated, and [^{3}C*] for each sample solution was subsequently calculated using Eq. (12). The calculated [^{3}C*] values were also corrected using S_λ (Eq. 6) of the extract solution.

2.3 $PM_{2.5}$ composition analysis and auxiliary measurements

The chemical composition of $PM_{2.5}$ (including WSOC, organic source tracers, and water-soluble ions) was analyzed to evaluate its role in photooxidant formation under irradiation. WSOC fractions including total WSOC, moderately hydrophilic WSOC (MH-WSOC), and strongly hydrophilic WSOC (SH-WSOC) were quantified using a carbon analyzer (Shimadzu TOC-L CPN) following appropriate extraction and isolation pretreatments (Yu et al., 2021a). Seven source-specific organic tracers were analyzed by GC/MS/MS (Shimadzu TQ 8040), including primary markers (levoglucosan for biomass burning, cholesterol for cooking) and secondary SOA tracers (phthalic acid for aromatic SOA, 4-methyl-5-nitrocatechol for aged biomass burning SOA, cis-pinonic acid for fresh biogenic SOA, and 2-methylerythritol plus 3-hydroxyglutaric acid for aged biogenic SOA). Water-soluble ions (NO_3^-, NO_2^-, Fe^{2+}, an Fe^{3+}) relevant to photo-oxidant formation were determined by ion chromatography (Dionex 600). The detailed analytical procedures are provided in our previous work (Yu et al., 2021a; 2022).

The aerosol water content of $PM_{2.5}$ during the sampling period was computationally determined using the ISORROPIA-II thermodynamic equilibrium model (Guo et al., 2015; Pye et al., 2020). The concurrent meteorological data (temperature, relative humidity, wind speed, solar radiation, and precipitation) were

https://doi.org/10.5194/egusphere-2026-2792
Preprint. Discussion started: 21 July 2026

acquired at 5-minute intervals by an automated HOBO weather monitoring system, and were averaged over 12 hours to align with the $PM_{2.5}$ sampling protocol.

3 Results and discussion

3.1 Steady-state concentrations of photooxidants in $PM_{2.5}$ extracts

3.1.1 Formation rate, loss rate, and steady-state concentration of ·OH

As shown in Fig. 1a, the formation rate (P_{OH}) and loss rate constant (k'_{OH}) of ·OH in irradiated aqueous $PM_{2.5}$ extracts showed greater seasonal variability than its steady state concentration [·OH]. In fact, P_{OH} and k'_{OH} aligned well with the mass concentration variations of WSOC (Fig. S2), which could be attributable to the dual role of WSOC as both a primary source and major sink for ·OH (see Sect. 3.2 for detailed discussion). The measured mean values of P_{OH} and k'_{OH} were (6.59 ± 7.12) × 10^{-10} M·s^{-1} and (2.97 ± 2.40) × 10^{5} s^{-1}, respectively. Moreover, the organic carbon-normalized ·OH loss rate constant, $k'_{C,OH}$, was calculated as (3.5 ± 1.7) × 10^{8} L·(mol C) $^{-1}$·s^{-1}, which was comparable to that ((3.8 ± 1.9) × 10^{8} L·(mol C) $^{-1}$·s^{-1}) reported by Arakaki et al. (2013). The mean $k'_{C,OH}$ values in summer, autumn, and winter were (2.8 ± 1.1) × 10^{8}, (4.0 ± 1.4) × 10^{8}, and (3.7 ± 2.3) × 10^{8} L·(mol C) $^{-1}$·s^{-1}, respectively, indicating enhanced WSOC reactivity with ·OH in aerosol liquid water during autumn and winter. The mean [·OH] measured in $PM_{2.5}$ extracts was (1.82 ± 0.88) × 10^{-15} M, with seasonal values of (1.65 ± 0.44) × 10^{-15} M in summer, (1.94 ± 0.91) × 10^{-15} M in autumn, and (1.87 ± 1.17) × 10^{-15} M in winter. No statistically significant seasonal differences were observed ($p > 0.05$).

https://doi.org/10.5194/egusphere-2026-2792
Preprint. Discussion started: 21 July 2026

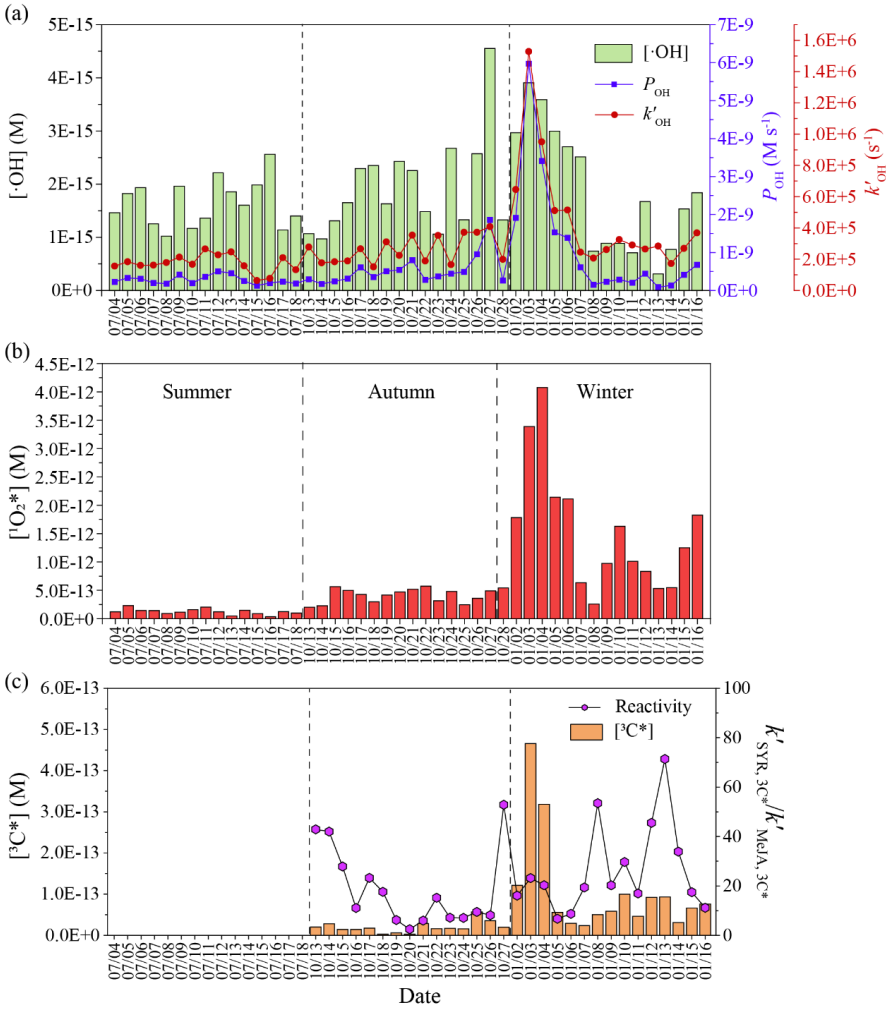

Figure 1. Seasonal variations in **(a)** the formation rate, loss rate constant, and steady-state concentration of ·OH; **(b)** steady-state concentration of $^1O_2$*; and **(c)** steady-state concentration and reactivity of ^{3}C* in irradiated aqueous $PM_{2.5}$ extracts (7.5 μg $PM_{2.5}$/mg H_2O).

3.1.2 Steady-state concentration of $^1O_2$*

As shown in Fig. 1b, the steady state concentration of $^1O_2$* exhibited greater seasonal variability than ·OH, with a mean value of (6.85 ± 0.87) × 10^{-13} M. While the

https://doi.org/10.5194/egusphere-2026-2792
Preprint. Discussion started: 21 July 2026

concentrations of ·OH and $^1O_2$* were consistent in magnitude with literature values, the annual mean [$^1O_2$*]/[·OH] ratio in this study was 376, slightly higher than that reported for Colorado (261; Leresche et al., 2021) but lower than that observed in California (~1000; Jiang et al., 2023; Ma et al., 2024). The seasonal [$^1O_2$*] means were (1.25 ± 0.52) × 10^{-13} M in summer, (4.14 ± 1.24) × 10^{-13} M in autumn, and (1.53 ± 1.08) × 10^{-12} M in winter, exhibiting statistically significant seasonal differences ($p < 0.05$). Notably, the steady-state concentration of $^1O_2$* in winter was substantially higher than that in summer and autumn. The seasonal [$^1O_2$*]/[·OH] ratios were 76, 213, and 818 for summer, autumn, and winter, respectively, indicating that $^1O_2$* played a more prominent role in aerosol aqueous-phase oxidation during winter, whereas ·OH contributed more significantly to summer aerosol oxidation.

3.1.3 Steady-state concentration and reactivity of ^{3}C*

The steady-state concentration and reactivity of ^{3}C* in irradiated $PM_{2.5}$ extracts were estimated from the decay rates of two probes, SYR and MeJA. As shown in Table S1, after correction for contributions from ·OH and $^1O_2$*, the pseudo-first-order rate constants for ^{3}C* reaction with SYR ($k'_{SYR,3C*}$) were (4.85 ± 3.21) × 10^{-5} s^{-1}, (7.09 ± 8.15) × 10^{-5} s^{-1}, and (2.79 ± 4.10) × 10^{-4} s^{-1} in summer, autumn, and winter, respectively, and the contributions of ^{3}C* oxidation to the total SYR decay rate (k'_{SYR}) were 48.5%, 50.6%, and 63.1%, respectively. Meanwhile, for MeJA, the $k'_{MeJA,3C*}$ values were (6.25 ± 6.48) × 10^{-6} s^{-1} and (1.92 ± 2.12) × 10^{-5} s^{-1} for autumn and winter, respectively, accounting for 31.7% and 56.8% to the total MeJA decay rate; the summer contribution was negligible. These results demonstrated that the importance of ^{3}C* in oxidizing

https://doi.org/10.5194/egusphere-2026-2792
Preprint. Discussion started: 21 July 2026

organic precursors followed the order of winter > autumn > summer. Furthermore, the ratios of $k'_{SYR,3C*}$ and $k'_{MeJA,3C*}$ to WSOC mass concentrations ($k'_{SYR,3C*}$/[WSOC] and $k'_{MeJA,3C*}$/[WSOC]) also exhibited the order of winter > autumn > summer, consistent with the findings of Chen et al. (2021). This suggested stronger ^{3}C* generation per unit WSOC mass in winter, while the lower summer value likely reflected photobleaching or degradation of water-soluble BrC under intense solar radiation (Lei et al., 2025). Thus, ^{3}C* photogenerated from BrC could significantly oxidize organic precursors and promote SOA formation in autumn and winter, which is an important SOA formation mechanism that has been overlooked in previous model simulations.

The ratio of pseudo-first-order rate constants for ^{3}C* reaction with SYR and MeJA ($k'_{SYR,3C*}/k'_{MeJA,3C*}$) indicates the average reactivity of ^{3}C*: values approaching unity denote higher reactivity, while elevated values signify lower reactivity (Kaur and Anastasio, 2018; Kaur et al., 2019). As shown in Fig. 1c, the ratio of $k'_{SYR,3C*}/k'_{MeJA,3C*}$ for all samples ranged from 2.5 to 71.4, intermediate between that with triplet benzophenone (^{3}BP*, 1.7) and triplet 2-acetonaphthone (^{3}2-AN*, 100). The mean ratios were 18.6 $\pm$ 15.9 in autumn and 26.3 $\pm$ 18.0 in winter, showing relatively higher reactivity of ^{3}C* in autumn than in winter. The average reactivity of ^{3}C* photogenerated from $PM_{2.5}$ extracts in this study was comparable to that observed in California during winter (Kaur et al., 2019; Ma et al., 2023). However, the ^{3}C* reactivity of $PM_{2.5}$ extracts in this study showed broader range across all samples than that observed in California, likely due to larger sample size and greater pollution variation. Besides, the autumn and winter means of [^{3}C*] were (1.97 ± 1.33) × 10^{-14} M and (1.08 ± 1.22) × 10^{-13} M,

https://doi.org/10.5194/egusphere-2026-2792
Preprint. Discussion started: 21 July 2026

respectively, yielding a [·OH]: [$^1O_2$*]: [^{3}C*] ratio of 1: 213: 10 in autumn and 1: 818: 58 in winter. Compared to the ratio reported in the California winter study (1: 290: 170), the winter $PM_{2.5}$ extracts collected in Beijing produced significantly more $^1O_2$* upon irradiation, whereas the relative importance of ^{3}C* was less pronounced than in California (Ma et al., 2023).

3.2 Influencing factors of photooxidants in $PM_{2.5}$ aqueous phase

3.2.1 Influencing factors of ·OH

The photoproduction pathways of ·OH in aerosol aqueous-phase primarily include photolysis of NO_2^-, NO_3^-, H_2O_2, and organic peroxides; photo-Fenton reactions; and photogeneration from WSOC (Mcneill, 2015; Li et al., 2023; Sun et al., 2024). Previous studies in California showed that NO_2^- and NO_3^- photolysis contributed approximately 70%–90% to ·OH photoproduction in winter fog droplets and approximately 34% in $PM_{2.5}$ extracts (Kaur et al., 2019; Kaur and Anastasio, 2018). In our $PM_{2.5}$ extracts (Fig. S3), NO_2^- photolysis contributed 4.5%, 8.4%, and 0.7% to ·OH production ($P_{OH, NO2-}/P_{OH}$) in summer, autumn, and winter, respectively, while NO_3^- photolysis ($P_{OH, NO3-}/P_{OH}$) contributed 11.1%, 20.8%, and 7.3%, which were significantly lower than California values. To quantify the impact of other sources on ·OH formation, $P_{OH, Other}$ was calculated by subtracting $P_{OH, NO2-}$ and $P_{OH, NO3-}$ from P_{OH}. As shown in Fig. 2, $P_{OH, Other}$ correlated strongly with WSOC concentration ($r = 0.89$, $p < 0.001$), moderately hydrophilic WSOC (MH-WSOC, $r = 0.78$), and strongly hydrophilic WSOC (SH-WSOC, $r = 0.81$). Further correlation analysis revealed significant associations between $P_{OH, Other}$ and anthropogenic tracers: levoglucosan ($r = 0.71$), phthalic acid ($r =$

https://doi.org/10.5194/egusphere-2026-2792
Preprint. Discussion started: 21 July 2026

0.79), and methylnitrocatechol ($r = 0.57$) ($p < 0.001$), but not with biogenic tracers (e.g., cis-pinonic acid, $r = 0.11$; $p > 0.05$). Water-soluble iron (WS-Fe, $r = 0.64$, $p < 0.001$) also showed strong correlation, implicating its role in ·OH generation.

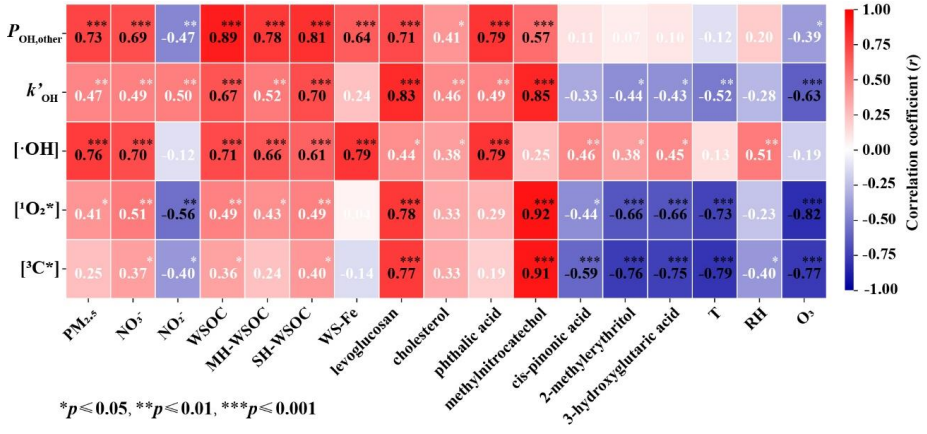

Figure 2. Correlation coefficients of ·OH photoproduction rate ($P_{OH, Other}$), ·OH loss rate constant (k'_{OH}), and steady-state concentrations of the three oxidants ([·OH], [$^1O_2$*], and [^3C*]) in irradiated aqueous $PM_{2.5}$ extracts with chemical species in $PM_{2.5}$ as well as meteorological conditions.

Organic matter can act as both the primary source and sink for ·OH in $PM_{2.5}$ extracts (Zhang et al., 2024). In this study, k'_{OH} showed a strong positive correlation with WSOC concentration, especially with SH-WSOC ($r = 0.70$, $p < 0.001$). However, correlation analysis between k'_{OH} and organic tracers (Fig. 2) revealed markedly different patterns: k'_{OH} correlated strongly with biomass burning tracers including levoglucosan ($r = 0.83$, $p < 0.001$) and methylnitrocatechol ($r = 0.85$, $p < 0.001$), but weakly or negatively with biogenic tracers including cis-pinonic acid ($r = -0.33$, $p > 0.05$), 2-methylerythritol ($r = -0.44$, $p < 0.05$), and 3-hydroxyglutaric acid ($r = -0.43$, $p < 0.05$). This demonstrates that anthropogenic organic matter, particularly that

https://doi.org/10.5194/egusphere-2026-2792
Preprint. Discussion started: 21 July 2026

from biomass burning, is efficient in ·OH scavenging, while biogenic contributions are negligible or inhibitory.

The primary factors influencing the steady state concentration of ·OH were further analyzed. Figure 3 shows [·OH] in irradiated aqueous $PM_{2.5}$ extracts as functions of NO_3^-, WS-Fe, and WSOC concentrations. As shown in Fig. 3a, [·OH] increased progressively with NO_3^- concentration, since NO_3^- photolysis generates ·OH without consuming it. Similarly, [·OH] rose gradually with WS-Fe concentration (Fig. 3b), attributable to iron ions promoting ·OH formation via Fenton and photo-Fenton reactions without significant scavenging. Figure 3c reveals a positive correlation between [·OH] and WSOC concentration, however, [·OH] plateaued at higher WSOC levels, due to balanced ·OH formation and consumption rates.

The effects of meteorological conditions on [·OH] were also investigated. As shown in Fig. 2, neither temperature (T; $r = 0.13$, $p > 0.05$) nor O_3 concentration ($r = -0.19$, $p > 0.05$) correlated significantly with [·OH], while relative humidity (RH) showed a relatively strong positive correlation ($r = 0.51$, $p < 0.01$). Table S2 reveals that RH correlated more strongly with NO_3^-, WS-Fe, and WSOC concentrations than did T or O_3, explaining RH's greater influence on [·OH] levels.

https://doi.org/10.5194/egusphere-2026-2792
Preprint. Discussion started: 21 July 2026

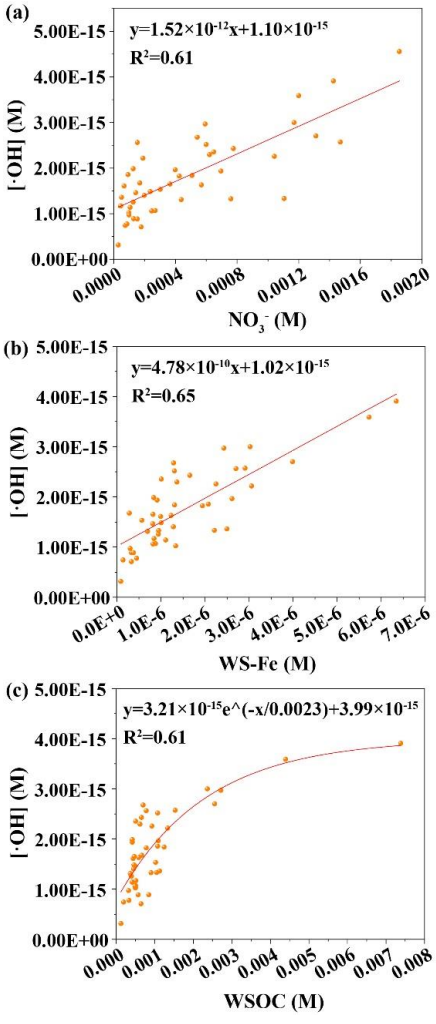

Figure 3. The steady-state concentration of ·OH in irradiated aqueous $PM_{2.5}$ extracts as functions of **(a)** NO_3^- concentration, **(b)** WS-Fe concentration, and **(c)** WSOC concentration.

3.2.2 Influencing factors of $^1O_2$* and ^{3}C*

$^1O_2$* is generated through energy transfer from photoexcited water-soluble organic chromophores (forming ^{3}C*) to ground-state O_2 (Ma et al., 2023; Li et al., 2023). Consequently, [$^1O_2$*] and [^{3}C*] showed similar correlation pattern with the investigated

https://doi.org/10.5194/egusphere-2026-2792
Preprint. Discussion started: 21 July 2026

factors (Fig. 2). While Kaur et al. (2019) reported a strong correlation between [$^1O_2$*] and WSOC (R^2 = 0.94, p < 0.01) in California winter $PM_{2.5}$ extracts, our study shows weaker but still significant correlations for both [$^1O_2$*] (r = 0.49, p < 0.01) and [^3C*] (r = 0.36, p < 0.05) with WSOC. Notably, both species exhibited strong positive correlations exclusively with biomass burning tracers including levoglucosan ($^1O_2$*: r = 0.78, ^3C*: r = 0.77; p < 0.001) and methylnitrocatechol ($^1O_2$*: r = 0.92, ^3C*: r = 0.91; p < 0.001), indicating that WSOC from primary biomass burning emissions and subsequent secondary formation contributes highly to ^3C* and $^1O_2$* production. This is consistent with the strong light absorption by nitroaromatic compounds and phenolic oxidation products from biomass burning in the near-UV and visible regions (Lei et al., 2025), which efficiently promotes ^3C* excitation and subsequent $^1O_2$* formation.

In contrast, biogenic SOA typically exhibits weak light absorption at 300–500 nm and minimal ^3C* and $^1O_2$* generation upon irradiation (Manfrin et al., 2019). Additionally, increasing temperature and O_3 concentration likely enhance both photobleaching of water-soluble BrC under intense solar radiation (Lei et al., 2025) and quenching of ^3C* and $^1O_2$* in the aqueous phase, resulting in strong negative correlations of T and O_3 with ^3C* and $^1O_2$*. The combined effects of high temperature, elevated O_3 concentration, and substantial contribution of biogenic SOA to WSOC in summer therefore explain the significantly lower [^3C*] and [$^1O_2$*] observed in summer compared to winter in this study.

Overall, the distinct correlation patterns observed between the three oxidants and chemical species in $PM_{2.5}$ provide critical insights into their formation mechanisms.

https://doi.org/10.5194/egusphere-2026-2792
Preprint. Discussion started: 21 July 2026

The particularly significant associations of [$^1O_2$*] and [^{3}C*] with biomass burning tracers suggest that these oxidants are predominantly generated via the photoexcitation of chromophoric dissolved organic matter derived from biomass combustion (Kuang et al., 2020; Jiang et al., 2023). In contrast, the strong correlations of [·OH] with NO_3^-, WS-Fe, and WSOC indicate a more complex origin, driven by diverse aqueous-phase photochemical pathways, including nitrate photolysis and Fenton-like reactions involving transition metals (Ervens, 2022). This mechanistic divergence aligns well with previous findings (Kuang et al., 2020; Jiang et al., 2023), underscoring the unique role of biomass-derived chromophores in sustaining [$^1O_2$*] and [^{3}C*] compared to the multifaceted sources of [·OH].

3.3 Estimation of photooxidant concentrations in aerosol liquid water

3.3.1 Effect of extract concentration on photooxidant steady-state concentrations

According to the ISORROPIA-II model calculation, the mean ambient aerosol water content in Beijing during the study period was 106.2 ± 348.0 μg·m^{-3}, corresponding to a mean $PM_{2.5}/H_2O$ ratio of 8.23 ± 11.78 μg $PM_{2.5}$/μg H_2O. Accordingly, the maximum $PM_{2.5}$ extract concentration used in this study (7.5 μg $PM_{2.5}$/mg H_2O) was three orders of magnitude lower than this ambient ratio. To examine extract concentration effects on photooxidant steady-state concentrations, we serially diluted the stock solution (7.5 μg $PM_{2.5}$/mg H_2O) and measured the steady-state concentrations of ·OH, $^1O_2$*, and ^{3}C* at various dilutions, so as to establish the functional relationships between photooxidant concentrations and extract concentration.

As shown in Fig.4, [$^1O_2$*], [^{3}C*], and [·OH] followed power-function growth with

https://doi.org/10.5194/egusphere-2026-2792
Preprint. Discussion started: 21 July 2026

460 increasing extract concentration, exhibiting similar trend profiles. The observed
461 relationship between [^{3}C*] and extract concentration aligned with the findings by Kaur
462 et al. (2019). While [^{3}C*] formation increased linearly with WSOC concentration,
463 elevated WSOC levels also induced ^{3}C* quenching (Wenk et al., 2013; Arciva et al.,
464 2024), leading to progressively slower [^{3}C*] growth. The parallel concentration profiles
465 of [$^1O_2$*] and [^{3}C*] were mechanistically consistent, as $^1O_2$* forms via energy transfer
466 from ^{3}C* to ground-state O_2 (Ossola et al., 2021). Notably, unlike our results, Kaur et
467 al. (2019) found no significant correlation between [·OH] and extract concentration.
468 This discrepancy reflects substantial differences in $PM_{2.5}$ composition between Beijing
469 and California, resulting in distinct dominant ·OH generation pathways under
470 irradiation.

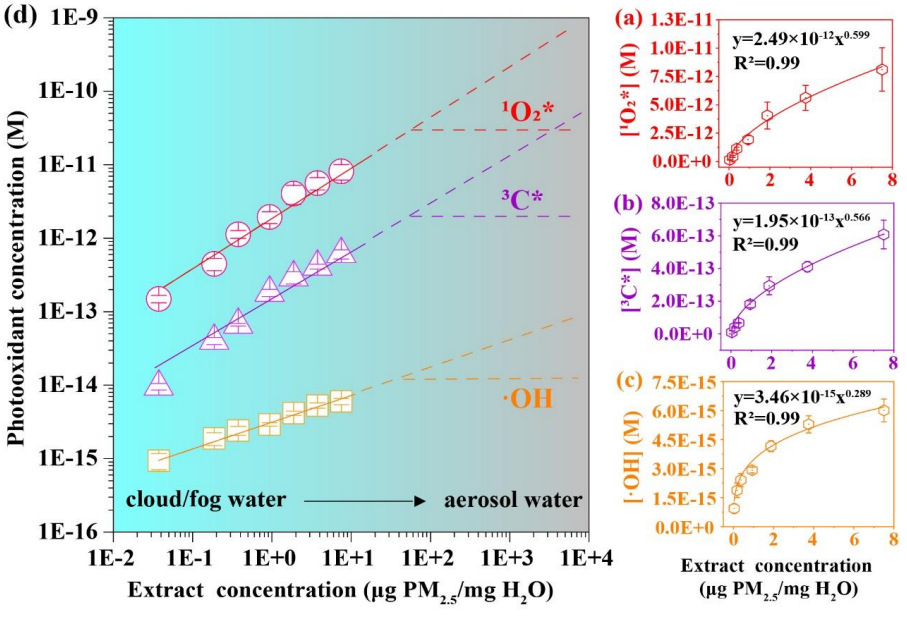

471

472 **Figure 4.** The steady-state concentrations of **(a)** $^1O_2$*, **(b)** ^{3}C*, and **(c)** ·OH as a function
473 of $PM_{2.5}$ extract concentration, and **(d)** the estimated concentration ranges of the three

https://doi.org/10.5194/egusphere-2026-2792
Preprint. Discussion started: 21 July 2026

photooxidants in cloud/fog water and aerosol water.

3.3.2 Estimation of steady-state concentrations of ·OH, $^1O_2$*, and ^3C* in aerosol liquid water

Given the substantial similarity in chemical composition between $PM_{2.5}$ extracts in this study and cloud/fog droplets, and the overlapping concentration ranges with cloud/fog water components (Kaur and Anastasio, 2017), our fitting curves reasonably represent photooxidant variations in cloud/fog droplets. As shown in Fig. 4d, the steady-state concentrations of photochemically generated oxidants in cloud/fog droplets followed the order of $[^1O_2^*] > [^3C^*] > [\cdot OH]$, where $[^1O_2^*]$ exceeded $[^3C^*]$ by 10-20 times and surpassed $[\cdot OH]$ by 2-3 orders of magnitude. As droplet chemical concentrations increase, $[^1O_2^*]$ and $[^3C^*]$ rise rapidly while $[\cdot OH]$ shows slower growth.

The steady-state photooxidant concentrations in atmospheric aerosol liquid water were further estimated through extrapolation. While Kaur et al. (2019) directly extrapolated fitted curves to determine oxidant concentration ranges, this approach carries significant uncertainty. As $PM_{2.5}/H_2O$ increases, certain water-soluble $PM_{2.5}$ components (e.g., $HULIS_{WS}$) reach saturation solubility, causing photooxidant concentration growth rates to decelerate and deviate from extrapolated curves. This suggests that Kaur's method may overestimate oxidant levels. We therefore applied this method conservatively, extending fitted curves to $PM_{2.5}/H_2O = 10^4$ μg/mg as upper concentration limits. As shown in Fig. 4d, we established lower limits by assuming saturation occurs at $PM_{2.5}/H_2O = 40$ μg/mg, where less soluble organic compounds cease dissolving and photooxidant concentrations plateau. Substitution into the fitting

https://doi.org/10.5194/egusphere-2026-2792
Preprint. Discussion started: 21 July 2026

equations in Figs. 4a–c yielded the following ranges for photochemically generated oxidants in atmospheric aerosol liquid water: [·OH] = (1.0–5.4) × 10^{-14} M, [$^1O_2$*] = (2.3–61.9) × 10^{-11} M, and [^{3}C*] = (1.6–35.8) × 10^{-12} M. In comparison, summer–winter measurements in Davis, California (following Kaur et al., 2019) reported estimated molar concentrations in aerosol liquid water on the order of 10^{-14} M for ·OH, 10^{-12}–10^{-11} M for $^1O_2$*, and 10^{-13}–10^{-12} M for ^{3}C* (Ma et al., 2024). Similarly, winter measurements in Fairbanks, Alaska reported estimated concentrations of up to 5× 10^{-15} M for ·OH, 3× 10^{-11} M for $^1O_2$* and 2× 10^{-12} M for ^{3}C* (Heinlein et al., 2025). These values are generally consistent with our predictions.

For ambient aerosol liquid water, despite the considerable uncertainties associated with extrapolated oxidant concentrations, it is relatively certain that [^{3}C*] exceeds [·OH] by 2–3 orders of magnitude, and [$^1O_2$*] exceeds [·OH] by 3–4 orders of magnitude. Therefore, although $^1O_2$* and ^{3}C* exhibit lower reactivity than ·OH and $^1O_2$* is highly selective (Manfrin et al., 2019), $^1O_2$* and ^{3}C* may still play important roles in aerosol aqueous-phase oxidation processes. Notably, compared to cloud/fog droplets, $^1O_2$* and ^{3}C* play more prominent roles than ·OH in atmospheric aerosol liquid water due to their substantially higher relative concentrations (Fig. 4).

4 Conclusions and atmospheric implications

Previous field observations in Beijing winter revealed elevated SOA concentrations with increasing SOC/OC ratios under heavy pollution (Yu et al., 2021a; 2021b). While weak solar radiation during winter/haze episodes typically maintains low gaseous oxidant levels, this raises the question: what oxidants drive substantial SOA

https://doi.org/10.5194/egusphere-2026-2792
Preprint. Discussion started: 21 July 2026

formation under these conditions? Through experimental approaches, we evaluated the importance of photooxidants in aerosol liquid water for precursor oxidation and SOA formation, aiming to identify missing oxidant sources during winter pollution episodes. The steady-state concentrations of three major photooxidants (·OH, $^1O_2$*, and ^{3}C*) in seasonal $PM_{2.5}$ extracts under simulated sunlight were quantified, and their controlling factors were analyzed. While biomass-burning-derived WSOC (both primary and secondary) dominated ^{3}C* and $^1O_2$* production, ·OH generation involved multiple sources (NO_3^-, WS-Fe, and diverse WSOC). Notably, [$^1O_2$*] and [^{3}C*] showed strong negative correlations with temperature and O_3, whereas ·OH exhibited weak correlations with these parameters. Seasonally, ·OH dominated summer aqueous-phase oxidation, while $^1O_2$* and ^{3}C* became more important in autumn/winter, which potentially explains the winter SOA formation paradox.

Our analysis of the functional relationships between photooxidant concentrations and $PM_{2.5}$ extract concentration revealed that [·OH], [$^1O_2$*], and [^{3}C*] all followed power-law growth patterns with increasing extract concentration, though with progressively decreasing growth rates. In ambient aerosol liquid water, [^{3}C*] concentrations exceeded [·OH] by 2-3 orders of magnitude, while [$^1O_2$*] surpassed [·OH] by 3-4 orders of magnitude. Consequently, despite their lower reactivities compared to ·OH, the substantially higher steady-state concentrations of both $^1O_2$* and ^{3}C* suggest that they could play significant roles in atmospheric aqueous-phase oxidation processes.

To further investigate the relative contributions of the three oxidants to ambient

https://doi.org/10.5194/egusphere-2026-2792
Preprint. Discussion started: 21 July 2026

aqueous-phase oxidation, we selected typical organic precursors and compared their aqueous oxidation pathways based on the estimated steady-state oxidant concentrations (derived from Fig. 4) and second-order rate constants (Table S3). The precursors included biomass burning emissions such as phenol, resorcinol, hydroquinone, eugenol, and vanillin, which exhibit high SOA formation potential (Li et al., 2023). We also examined green leaf volatiles, including methyl jasmonate, methyl salicylate, foliate acetate, cis-3-hexen-1-ol, and 2-methyl-3-buten-2-ol, primarily emitted from vegetation (Richards-Henderson et al., 2014). Using a cloud droplet concentration of 0.5 μg $PM_{2.5}$/mg H_2O, the steady-state oxidant concentrations were calculated as [·OH] = 2.8×10^{-15} M, [$^1O_2$*] = 1.6×10^{-12} M, and [^{3}C*] = 1.3×10^{-13} M. For aerosol liquid water, intermediate values between upper and lower estimates were used, yielding [·OH] = 3.2×10^{-14} M, [$^1O_2$*] = 3.0×10^{-10} M, and [^{3}C*] = 2.4×10^{-11} M.

Figure 5 shows the contributions of each oxidant (·OH, $^1O_2$*, and ^{3}C*) to aqueous-phase oxidation of typical precursors in cloud droplets and aerosol liquid water, calculated as the product of the steady-state oxidant concentrations and second-order rate constants. In cloud droplets, ^{3}C* dominates the oxidation of most precursors except *cis*-3-hexen-1-ol and 2-methyl-3-buten-2-ol, where ·OH is the primary oxidant. In aerosol liquid water, ^{3}C* drives the aqueous-phase oxidation of all precursors, while $^1O_2$* plays a significantly enhanced role and the role of ·OH is minor. In addition, previous studies have demonstrated that the aqueous-phase reaction rates of phenolic compounds and green leaf volatiles with ^{3}C* are temperature-independent Mcneill, 2015; Li et al., 2023). The negative correlation between ^{3}C* and temperature further

https://doi.org/10.5194/egusphere-2026-2792
Preprint. Discussion started: 21 July 2026

implies that $^{3}C^{*}$-mediated SOA formation could remain efficient even at low winter temperatures.

In summary, although $^{1}O_{2}^{*}$ and $^{3}C^{*}$ exhibit lower reactivities than ·OH, both species significantly contribute to aqueous-phase organic precursor oxidation and SOA formation, particularly in aerosol liquid water with elevated concentrations of chromophoric dissolved organic matter (Kuang et al., 2020; Jiang et al., 2023). While the volatility basis set and two-product approaches have been widely used for SOA simulation, previous studies have largely focused on ·OH as the most powerful atmospheric oxidant, attributing SOA formation primarily to ·OH-driven oxidation reactions (McVay and Ervens, 2017; Zhang et al., 2023). Current model simulations frequently overlook aerosol aqueous-phase processes, particularly lacking $^{1}O_{2}^{*}$ and $^{3}C^{*}$ mediated oxidation mechanisms. This omission possibly explains the systematic underestimation of SOA concentrations during winter and heavy pollution episodes.

As a significant source of $^{1}O_{2}^{*}$ and $^{3}C^{*}$, biomass burning emissions promote photochemical aqueous-phase SOA formation by increasing both photooxidant levels and precursor concentrations. Beyond SOA formation, $^{3}C^{*}$ may also drive secondary sulfate production in BrC-rich aerosols through surface reactions (Liang et al., 2024). Consequently, controlling biomass burning, such as crop residue combustion for cooking and heating in rural areas and wood burning for residential heating in Europe and North America, can substantially reduce ambient secondary aerosols by lowering VOC precursors and aqueous photooxidants, thereby suppressing subsequent oxidation (Heinlein et al., 2025). In this study, although the maximum $PM_{2.5}$ extract concentration

https://doi.org/10.5194/egusphere-2026-2792
Preprint. Discussion started: 21 July 2026

used (7.5 μg $PM_{2.5}$/mg H_2O) was approximately an order of magnitude higher than in previous research (Kaur et al., 2019; Ma et al., 2023, 2024), uncertainties remain in extrapolating photooxidant concentrations to ambient conditions because this value remained 2–3 orders of magnitude lower than typical ambient ratios. Future studies should therefore obtain more precise quantification of $^1O_2$* and ^{3}C* in biomass burning aerosols, and combine these data with model simulations to better assess their environmental impacts on the formation of secondary aerosols such as SOA and sulfate.

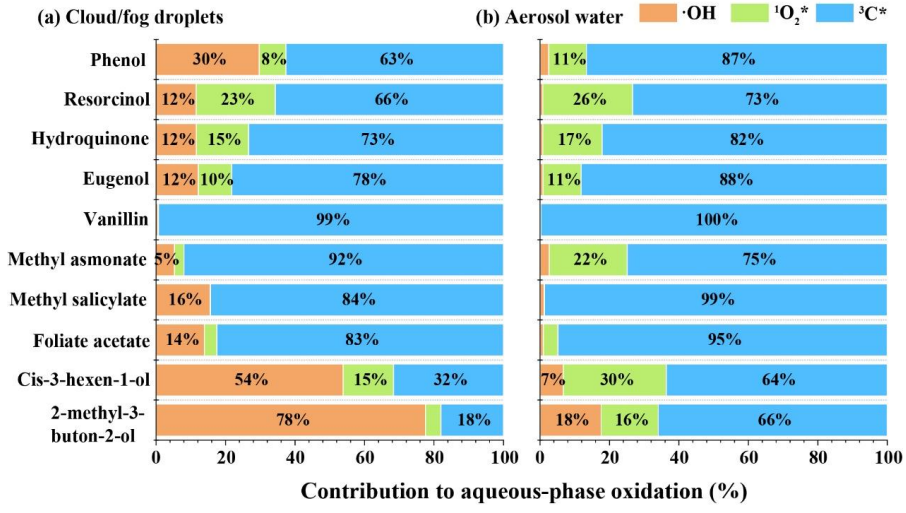

Figure 5. Contributions of ·OH, $^1O_2$*, and ^{3}C* to the aqueous-phase oxidation of typical organic precursors in cloud/fog droplets and aerosol liquid water.

Data availability.

The research data, which include the formation rates and loss rates of ·OH, the steady state concentrations of ·OH, $^1O_2$*, and ^{3}C*, as well as the concentrations of other related pollutants, are available at https://doi.org/10.5281/zenodo.20805514 (Cai et al., 2026).

https://doi.org/10.5194/egusphere-2026-2792
Preprint. Discussion started: 21 July 2026

Author contributions.

The manuscript was written through contributions of all authors. The corresponding author, JC, provided the ideas and funding, discussed the results, and revised the paper. The first author MC analyzed the data, plotted the figures, and wrote the manuscript. QY conducted the sampling and chemical analysis, analyzed the data, and put forward suggestions on the discussion. KX conducted the sampling and put forward suggestions on the discussion. MA conducted the sampling and put forward suggestions on the discussion.

Competing interests.

The authors declare that they have no conflict of interest.

Financial support. This work was financially supported by Jing-Jin-Ji Regional Integrated Environmental Improvement-National Science and Technology Major Project (2025ZD1204700), National Key R&D Program of China (2019YFC0214200), and National Natural Science Foundation of China (91543110).

References

Al-Abadleh, H. A.: Iron content in aerosol particles and its impact on atmospheric chemistry, Chem. Commun., 60, 1840-1855, https://doi.org/10.1039/d3cc04614a, 2024.

Arakaki, T., Anastasio, C., Kuroki, Y., Nakajima, H., Okada, K., Kotani, Y., Handa, D., Azechi, S.,

https://doi.org/10.5194/egusphere-2026-2792
Preprint. Discussion started: 21 July 2026

Kimura, T., Tsuhako, A., and Miyagi, Y.: A general scavenging rate constant for reaction of hydroxyl radical with organic carbon in atmospheric waters, Environ. Sci. Technol., 47, 8196-8203, https://doi.org/10.1021/es401927b, 2013.

Arciva, S., Ma, L., Mavis, C., Guzman, C., and Anastasio, C.: Formation and loss of light absorbance by phenolic aqueous SOA by ·OH and an organic triplet excited state, Atmos. Chem. Phys., 24, 4473-4485, https://doi.org/10.5194/acp-24-4473-2024, 2024.

Cai, M., Yu, Q., Xin, K., Ahmad, M., and Chen, J.: Seasonal dynamics and driving factors of aqueous-phase photooxidants in atmospheric particles: Implications for wintertime SOA formation, Zenodo [data set], https://doi.org/10.5281/zenodo.20805514, 2026.

Chen, Q., Mu, Z., Xu, L., Wang, M., Wang, J., Shan, M., Fan, X., Song, J., Wang, Y., Lin, P., and Du, L.: Triplet-state organic matter in atmospheric aerosols: Formation characteristics and potential effects on aerosol aging, Atmos. Environ., 252, https://doi.org/10.1016/j.atmosenv.2021.118343, 2021.

Dwinandha, D., Zhang, B., and Fujii, M.: Prediction of reaction mechanism for OH radical-mediated phenol oxidation using quantum chemical calculation, Chemosphere, 291, 132763, https://doi.org/10.1016/j.chemosphere.2021.132763, 2022.

Ervens, B.: Average cloud droplet size and composition: Good assumptions for predicting oxidants in the atmospheric aqueous phase?, J. Phys. Chem. A, 126, 8295-8304, https://doi.org/10.1021/acs.jpca.2c05527, 2022.

Fahey, K. M., Sareen, N., Carlton, A. G., and Hutzell, W. T.: Updated in-cloud secondary aerosol production in the northern hemisphere predicted by the community multiscale air quality modeling system, ACS Earth Space Chem., https://doi.org/10.1021/acsearthspacechem.4c00370, 2025.

Gemayel, R., Emmelin, C., Perrier, S., Tomaz, S., Baboomian, V. J., Fishman, D. A., Nizkorodov, S. A.,

https://doi.org/10.5194/egusphere-2026-2792
Preprint. Discussion started: 21 July 2026

643 Dumas, S., and George, C.: Quenching of ketone triplet excited states by atmospheric halides, Environ.
644 Sci.: Atmos., 1, 31-44, https://doi.org/10.1039/d0ea00011f, 2021.
645 Gerritz, L., Wei, J., Fang, T., Wong, C., Klodt, A. L., Nizkorodov, S. A., and Shiraiwa, M.: Reactive
646 oxygen species formation and peroxide and carbonyl decomposition in aqueous photolysis of secondary
647 organic aerosols, Environ. Sci. Technol., 58, 4716-4726, https://doi.org/10.1021/acs.est.3c08662, 2024.
648 Guo, H., Xu, L., Bougiatioti, A., Cerully, K. M., Capps, S. L., Hite, J. R., Carlton, A. G., Lee, S. H.,
649 Bergin, M. H., Ng, N. L., Nenes, A., and Weber, R. J.: Fine-particle water and pH in the southeastern
650 United States, Atmos. Chem. Phys., 15, 5211-5228, https://doi.org/10.5194/acp-15-5211-2015, 2015.
651 Gweme, D. T. and Styler, S. A.: OH radical oxidation of organosulfates in the atmospheric aqueous phase,
652 The Journal of Physical Chemistry A, 128, 9462-9475, https://doi.org/10.1021/acs.jpca.4c02877, 2024.
653 Heinlein, L. M. D., He, J., Sunday, M. O., Guo, F., Campbell, J., Moon, A., Kapur, S., Fang, T., Edwards,
654 K., Cesler-Maloney, M., Burns, A. J., Dibb, J., Simpson, W., Shiraiwa, M., Alexander, B., Mao, J., Flynn
655 Iii, J. H., Stutz, J., and Anastasio, C.: Surprisingly robust photochemistry in subarctic particles during
656 winter: evidence from photooxidants, Atmos. Chem. Phys., 25, 9561-9581, https://doi.org/10.5194/acp-
657 25-9561-2025, 2025.
658 Jiang, W., Ma, L., Niedek, C., Anastasio, C., and Zhang, Q.: Chemical and light-absorption properties of
659 water-soluble organic aerosols in northern california and photooxidant production by brown carbon
660 components, ACS Earth Space Chem., 7, 1107-1119,
661 https://doi.org/10.1021/acsearthspacechem.3c00022, 2023.
662 Jiang, W., Yu, L., Yee, L., Chhabra, P., Seinfeld, J., Anastasio, C., and Zhang, Q.: Chemical differences
663 between phenolic secondary organic aerosol formed through gas-phase and aqueous-phase reactions,
664 ACS Earth Space Chem., 8, 2270-2283, https://doi.org/10.1021/acsearthspacechem.4c00204, 2024.

https://doi.org/10.5194/egusphere-2026-2792
Preprint. Discussion started: 21 July 2026

Kaur, R. and Anastasio, C.: Light absorption and the photoformation of hydroxyl radical and singlet oxygen in fog waters, Atmos. Environ., 164, 387-397, https://doi.org/10.1016/j.atmosenv.2017.06.006, 2017.

Kaur, R. and Anastasio, C.: First measurements of organic triplet excited states in atmospheric waters, Environ. Sci. Technol., 52, 5218-5226, https://doi.org/10.1021/acs.est.7b06699, 2018.

Kaur, R., Labins, J. R., Helbock, S. S., Jiang, W., Bein, K. J., Zhang, Q., and Anastasio, C.: Photooxidants from brown carbon and other chromophores in illuminated particle extracts, Atmos. Chem. Phys., 19, 6579-6594, https://doi.org/10.5194/acp-19-6579-2019, 2019.

Kroflič, A., Schaefer, T., Huš, M., Phuoc Le, H., Otto, T., and Herrmann, H.: OH radicals reactivity towards phenol-related pollutants in water: temperature dependence of the rate constants and novel insights into the [OH–phenol]˙ adduct formation, Phys. Chem. Chem. Phys., 22, 1324-1332, https://doi.org/10.1039/c9cp05533a, 2020.

Kuang, Y., He, Y., Xu, W., Yuan, B., Zhang, G., Ma, Z., Wu, C., Wang, C., Wang, S., Zhang, S., Tao, J., Ma, N., Su, H., Cheng, Y., Shao, M., and Sun, Y.: Photochemical aqueous-phase reactions induce rapid daytime formation of oxygenated organic aerosol on the north china plain, Environ. Sci. Technol., 54, 3849-3860, https://doi.org/10.1021/acs.est.9b06836, 2020.

Lei, R., Sha, Y., Meng, H., Huang, Y., Ye, J., Huang, D. D., Zhang, Y., Wu, Y., Li, Y., and Ge, X.: Aqueous phase photolysis of 4-nitrocatechol: Reaction kinetics, evolutions of chemical composition, light absorption and oxidation potential, Atmos. Environ., 343, https://doi.org/10.1016/j.atmosenv.2024.120981, 2025.

Leresche, F., Salazar, J. R., Pfotenhauer, D. J., Hannigan, M. P., Majestic, B. J., and Rosario-Ortiz, F. L.: Photochemical aging of atmospheric particulate matter in the aqueous phase, Environ. Sci. Technol.,

https://doi.org/10.5194/egusphere-2026-2792
Preprint. Discussion started: 21 July 2026

687 https://doi.org/10.1021/acs.est.1c00978, 2021.

688 Li, F., Zhou, S., Du, L., Zhao, J., Hang, J., and Wang, X.: Aqueous-phase chemistry of atmospheric
689 phenolic compounds: A critical review of laboratory studies, Sci. Total Environ., 856,
690 https://doi.org/10.1016/j.scitotenv.2022.158895, 2023.

691 Li, H., Wang, X., Zhong, J., Chu, B., Ma, Q., Zeng, X. C., Francisco, J. S., and He, H.: Mechanistic study
692 of the aqueous reaction of organic peroxides with HSO_3^- on the surface of a water droplet, Angew. Chem.
693 Int. Ed., 60, 20200-20203, https://doi.org/10.1002/anie.202105416, 2021.

694 Liang, Z., Zhou, L., Chang, Y., Qin, Y., and Chan, C. K.: Biomassburning organic aerosols as a pool of
695 atmospheric reactive triplets to drive multiphase sulfate formation, P. Natl. Acad. Sci. USA, 121,
696 e2416803121, https://doi.org/10.1073/pnas.2416803121, 2024.

697 Ma, L., Worland, R., Jiang, W., Niedek, C., Guzman, C., Bein, K. J., Zhang, Q., and Anastasio, C.:
698 Predicting photooxidant concentrations in aerosol liquid water based on laboratory extracts of ambient
699 particles, Atmos. Chem. and Phys., 23, 8805-8821, https://doi.org/10.5194/acp-23-8805-2023, 2023.

700 Ma, L., Worland, R., Heinlein, L., Guzman, C., Jiang, W., Niedek, C., Bein, K. J., Zhang, Q., and
701 Anastasio, C.: Seasonal variations in photooxidant formation and light absorption in aqueous extracts of
702 ambient particles, Atmos. Chem. Phys., 24, 1-21, https://doi.org/10.5194/acp-24-1-2024, 2024.

703 Mabato, B. R. G., Li, Y. J., Huang, D. D., Wang, Y., and Chan, C. K.: Comparison of aqueous secondary
704 organic aerosol (aqSOA) product distributions from guaiacol oxidation by non-phenolic and phenolic
705 methoxybenzaldehydes as photosensitizers in the absence and presence of ammonium nitrate, Atmos.
706 Chem. and Phys., 23, 2859-2875, https://doi.org/10.5194/acp-23-2859-2023, 2023.

707 Mabato, B. R. G., Lyu, Y., Ji, Y., Huang, D. D., Li, X., Nah, T., Lam, C. H., and Chan, C. K.: Aqueous
708 SOA formation from the photo-oxidation of vanillin: Direct photosensitized reactions and nitrate-

https://doi.org/10.5194/egusphere-2026-2792
Preprint. Discussion started: 21 July 2026

709 mediated reactions, Atmos. Chem. and Phys., https://doi.org/10.5194/acp-2021-396, 2021.

710 Mabato, B. R. G., Lyu, Y., Ji, Y., Li, Y. J., Huang, D. D., Li, X., Nah, T., Lam, C. H., and Chan, C. K.:
711 Aqueous secondary organic aerosol formation from the direct photosensitized oxidation of vanillin in the
712 absence and presence of ammonium nitrate, Atmos. Chem. and Phys., 22, https://doi.org/273-293,
713 10.5194/acp-22-273-2022, 2022.

714 Manfrin, A., Nizkorodov, S. A., Malecha, K. T., Getzinger, G. J., McNeill, K., and Borduas-Dedekind,
715 N.: Reactive oxygen species production from secondary organic aerosols: The importance of singlet
716 oxygen, Environ. Sci. Technol., 53, 8553-8562, https://doi.org/10.1021/acs.est.9b01609, 2019.

717 McNeill, V. F.: Aqueous organic chemistry in the atmosphere: sources and chemical processing of organic
718 aerosols, Environ. Sci. Technol., 49, 1237-1244, https://doi.org/10.1021/es5043707, 2015.

719 McVay, R. and Ervens, B.: A microphysical parameterization of aqSOA and sulfate formation in clouds,
720 Geophys. Res. Lett., 44, 7500-7509, https://doi.org/10.1002/2017gl074233, 2017.

721 Mitra, K., Mishra, H. R., Pei, X., and Pathak, R. K.: Secondary organic aerosol (SOA) from photo-
722 oxidation of toluene: 1 Influence of reactive nitrogen, acidity and water vapours on optical properties,
723 Atmosphere, 13, 1099, https://doi.org/10.3390/atmos13071099, 2022.

724 Ossola, R., Jönsson, O. M., Moor, K., and McNeill, K.: Singlet oxygen quantum yields in environmental
725 waters, Chem. Rev., 121, 4100-4146, https://doi.org/10.1021/acs.chemrev.0c00781, 2021.

726 Pye, H. O. T., Nenes, A., Alexander, B., Ault, A. P., Barth, M. C., Clegg, S. L., Collett Jr, J. L., Fahey, K.
727 M., Hennigan, C. J., Herrmann, H., Kanakidou, M., Kelly, J. T., Ku, I. T., McNeill, V. F., Riemer, N.,
728 Schaefer, T., Shi, G., Tilgner, A., Walker, J. T., Wang, T., Weber, R., Xing, J., Zaveri, R. A., and Zuend,
729 A.: The acidity of atmospheric particles and clouds, Atmos. Chem. Phys., 20, 4809-4888,
730 https://doi.org/10.5194/acp-20-4809-2020, 2020.

731 Richards-Henderson, N. K., Hansel, A. K., Valsaraj, K. T., and Anastasio, C.: Aqueous oxidation of green

https://doi.org/10.5194/egusphere-2026-2792
Preprint. Discussion started: 21 July 2026

leaf volatiles by hydroxyl radical as a source of SOA: Kinetics and SOA yields, Atmos. Environ., 95, 105-112, https://doi.org/10.1016/j.atmosenv.2014.06.026, 2014.

Sun, W., Zhang, G., Guo, Z., Fu, Y., Peng, X., Yang, Y., Hu, X., Lin, J., Jiang, F., Jiang, B., Liao, Y., Chen, D., Chen, J., Ou, J., Wang, X., Peng, P. a., and Bi, X.: Formation of in-cloud aqueous-phase secondary organic matter and related characteristic molecules, J. Geophys. Res.: Atmos., 129, https://doi.org/10.1029/2023jd040355, 2024.

Sun, Y., Yu, Q., Qin, W., Zhang, Y., Xin, K., Ai, J., and Chen, J.: Characteristics and plausible formation mechanisms of secondary inorganic and organic aerosols in four seasons and during haze episodes in Beijing, Atmos. Res., 316, https://doi.org/10.1016/j.atmosres.2025.107949, 2025.

Tilgner, A., Schaefer, T., Alexander, B., Barth, M., Collett Jr, J. L., Fahey, K. M., Nenes, A., Pye, H. O. T., Herrmann, H., and McNeill, V. F.: Acidity and the multiphase chemistry of atmospheric aqueous particles and clouds, Atmos. Chem. Phys., 21, 13483-13536, https://doi.org/10.5194/acp-21-13483-2021, 2021.

Tong, X., Wang, S., and Wang, L.: Kinetics and mechanism of syringic acid degradation initiated by hydroxyl radical and sulphate radical in the aqueous phase, Chemosphere, 256, 126997, https://doi.org/10.1016/j.chemosphere.2020.126997, 2020.

Wang, H., Sun, Y., and Dong, F.: Insight into the overlooked photochemical decomposition of atmospheric surface nitrates triggered by visible light, Angew. Chem. Int. Ed., 61, e202209201, https://doi.org/10.1002/anie.202209201, 2022a.

Wang, T., Li, K., Bell, D. M., Zhang, J., Cui, T., Surdu, M., Baltensperger, U., Slowik, J. G., Lamkaddam, H., El Haddad, I., and Prevot, A. S. H.: Large contribution of in-cloud production of secondary organic aerosol from biomass burning emissions, npj Clim. Atmos. Sci., 7, https://doi.org/10.1038/s41612-024-

https://doi.org/10.5194/egusphere-2026-2792
Preprint. Discussion started: 21 July 2026

00682-6, 2024.

Wang, Y., Jorga, S., and Abbatt, J.: Nitration of phenols by reaction with aqueous nitrite: A pathway for the formation of atmospheric brown carbon, ACS Earth Space Chem., 7, 632-641, https://doi.org/10.1021/acsearthspacechem.2c00396, 2023.

Wang, Y., Huang, W., Tian, L., Wang, Y., Li, F., Huang, D. D., Zhang, R., Go Mabato, B. R., Huang, R.-J., Chen, Q., Ge, X., Du, L., Ma, Y. G., Gen, M., Hoi, K. I., Mok, K. M., Yu, J. Z., Chan, C. K., Li, X., and Li, Y. J.: Decay kinetics and absorption changes of methoxyphenols and nitrophenols during nitrate-mediated aqueous photochemical oxidation at 254 and 313 nm, ACS Earth Space Chem., 6, 1115-1125, https://doi.org/10.1021/acsearthspacechem.2c00021, 2022b.

Wenk, J., Eustis, S. N., McNeill, K., and Canonica, S.: Quenching of excited triplet states by dissolved natural organic matter, Environ. Sci. Technol., 47, 12802-12810, https://doi.org/10.1021/es402668h, 2013.

Yu, Q., Chen, J., Qin, W., Cheng, S., Zhang, Y., Sun, Y., Xin, K., and Ahmad, M.: Characteristics, primary sources and secondary formation of water-soluble organic aerosols in downtown Beijing, Atmos. Chem. Phys., 21, 1775-1796, https://doi.org/10.5194/acp-21-1775-2021, 2021a.

Yu, Q., Chen, J., Cheng, S., Qin, W., Zhang, Y., Sun, Y., and Ahmad, M.: Seasonal variation of dicarboxylic acids in PM2.5 in Beijing: Implications for the formation and aging processes of secondary organic aerosols, Sci. Total Environ., 763, https://doi.org/10.1016/j.scitotenv.2020.142964, 2021b.

Yu, Q., Chen, J., Qin, W., Ahmad, M., Zhang, Y., Sun, Y., Xin, K., and Ai, J.: Oxidative potential associated with water-soluble components of PM2.5 in Beijing: The important role of anthropogenic organic aerosols, J. Hazard. Mater., 433, https://doi.org/10.1016/j.jhazmat.2022.128839, 2022.

Zhang, J., Shrivastava, M., Ma, L., Jiang, W., Anastasio, C., Zhang, Q., and Zelenyuk, A.: Modeling

https://doi.org/10.5194/egusphere-2026-2792
Preprint. Discussion started: 21 July 2026

776 novel aqueous particle and cloud chemistry processes of biomass burning phenols and their potential to
777 form secondary organic aerosols, Environ. Sci. Technol., 58, 3776-3786,
778 https://doi.org/10.1021/acs.est.3c07762, 2024.
779 Zhang, Y., Huang, H., Qin, W., Yu, Q., Sun, Y., Cheng, S., Ahmad, M., Ouyang, W., Soyol-Erdene, T.-
780 O., and Chen, J.: Modeling of wintertime regional formation of secondary organic aerosols around
781 Beijing: sensitivity analysis and anthropogenic contributions. Carbon Res., 2:6,
782 https://doi.org/10.1007/s44246-023-00040-w, 2023.
783